

Analytical Methods

Accepted Manuscript



This is an *Accepted Manuscript*, which has been through the Royal Society of Chemistry peer review process and has been accepted for publication.

Accepted Manuscripts are published online shortly after acceptance, before technical editing, formatting and proof reading. Using this free service, authors can make their results available to the community, in citable form, before we publish the edited article. We will replace this *Accepted Manuscript* with the edited and formatted *Advance Article* as soon as it is available.

You can find more information about *Accepted Manuscripts* in the [Information for Authors](#).

Please note that technical editing may introduce minor changes to the text and/or graphics, which may alter content. The journal's standard [Terms & Conditions](#) and the [Ethical guidelines](#) still apply. In no event shall the Royal Society of Chemistry be held responsible for any errors or omissions in this *Accepted Manuscript* or any consequences arising from the use of any information it contains.

1
2
3 **Application of vibrational spectroscopy techniques to non-destructively monitor plant**
4
5 **health and development**
6
7

8
9 Holly J. Butler^{ab}, Martin R. McAinsh^{c,*}, Steven Adams^d, Francis L. Martin^{a,*}
10

11
12 ^a*Centre for Biophotonics*, ^b*Centre for Global Eco-Innovation*, ^c*Lancaster Environment*
13
14 *Centre, Lancaster University, Lancaster LA1 4YQ, UK*; ^d*Plant Impact Plc, Rothamsted, West*
15
16 *Common, Harpenden, Hertfordshire AL5 2JQ, UK*
17
18
19
20
21
22
23
24
25
26
27
28
29
30
31
32

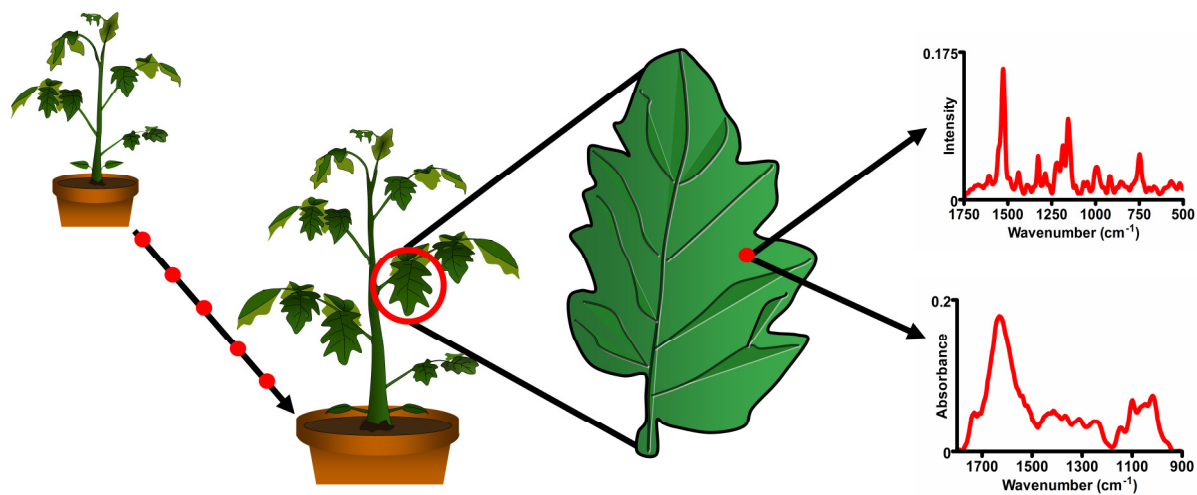
33 ***Correspondence to:** Prof Francis L Martin, Centre for Biophotonics, LEC, Lancaster
34
35 University, Lancaster LA1 4YQ, UK; Email: f.martin@lancaster.ac.uk; Tel.: +44(0)1524
36
37 510206
38
39

40
41 Dr Martin R McAinsh, Lancaster Environment Centre, Lancaster University, Lancaster LA1
42
43 4YQ, UK; Email: m.mcainsh@lancaster.ac.uk; Tel.: +44(0)1524 510553
44
45
46
47
48
49
50
51
52
53
54
55
56
57
58
59
60

Abstract

Vibrational spectroscopy is a powerful analytical tool that is yet to be fully developed in plant science. Previously, these tools have been primarily applied to fixed or *in vitro* biological materials, which do not effectively encapsulate real-time physiological conditions of whole organisms. Coupled with multivariate analysis, this study examines the potential application of ATR-FTIR or Raman spectroscopy to determine spectral alterations indicative of healthy plant growth in leaf samples of *Solanum lycopersicum*. This was achieved in the absence of destructive effects on leaf tissues locally or on plant health systemically; additionally, autofluorescence was not a confounder. Feature extraction techniques including PCA-LDA were employed to examine variance within spectral datasets. *In vivo* measurements are able to successfully characterise key constituents of the leaf cuticle and cell wall, whilst qualifying leaf growth. Major alterations in carbohydrate and protein content of leaves were observed, correlating with known processes within leaf development from cell wall expansion to leaf senescence. These findings show that vibrational spectroscopy is an ideal technique for *in vivo* investigations in plant tissues.

ToC graphic



Characterisation of plant leaf growth employing vibrational spectroscopy approaches.

Introduction

With an increasing population anticipated to reach 9 billion by 2050, it is estimated that agricultural productivity will need to increase by 70% in order to meet global food demands¹. For this reason, plant science and food security are prominent research topics that are fundamental to providing sustainable nutrition for the foreseeable future. There are powerful genomic, proteomic and physiological analysis tools available that have been widely implemented in plant research, yet many are invasive and destructive to the whole tissue. In particular, determination of the nutrient status of plant tissue is profoundly reliant upon chemical analyses, which often requires substantial sample preparation and training that can prove time-consuming and expensive². Plant-focused research remains limited due to a lack of analytical methods that can be applied in a truly non-destructive manner, that can convey both chemical and structural information *in vivo* across all plant species³.

It is evident that a high-throughput, cost effective and non-destructive technique would benefit the field of plant science and therefore food security. Vibrational spectroscopy in biological systems, or biospectroscopy, has been shown to be a valuable tool for exploratory analysis in the disciplines of ecotoxicology⁴⁻⁶, food science^{7, 8} and biomedical research⁹. The latter of these fields has expanded markedly in the past decade with research spanning pharmaceuticals¹⁰, cytology^{11, 12}, histopathology¹³⁻¹⁵ and cancer diagnostics in cervical¹⁶, prostate¹⁷, breast¹⁸ and mucosal¹⁹ tissues. This is in part associated with advancements in biospectroscopy that allows for non-invasive analysis of live cells and tissues²⁰, additional to biological fluids samples such as blood²¹, serum²² and plasma²³ that translate into a clinical setting. In comparison, vibrational spectroscopy has only been tentatively implemented across fundamental plant biology and agronomy to provide an insight into the microscopic and subcellular properties of plant tissues²⁴⁻²⁶. This could not only infer qualitative and

1
2
3 quantitative information regarding the biological components of the tissues in question, but
4
5 also any mechanical, environmental and nutritional stress that they are subjected to²⁷⁻²⁹.
6
7

8
9 Infrared (IR) and Raman spectroscopy are two complementary vibrational spectroscopy
10
11 methods that are commonly employed when investigating biological samples. Although
12
13 based on distinctly different physical processes, both observe the excitation of a molecule to
14
15 higher energy levels due to chemical bond absorption of radiation. IR spectroscopy uses
16
17 polychromatic light in the IR region that causes molecules within a sample to vibrate due to
18
19 their chemical composition³⁰. Coupled with the Fourier-transform (FT) algorithm conversion
20
21 of an interferogram, a spectrum is rapidly obtained as transmittance or absorption of energy
22
23 plotted against energy in wavenumbers. The consequent spectrum derived is indicative of the
24
25 chemical bonds present and therefore provides an insight into biochemical ‘fingerprint’ of the
26
27 sample³¹. FTIR spectroscopy in plant research has been limited due to the strong dipole
28
29 moment of water and thus investigations have been predominantly conducted in non-aqueous
30
31 and dried material³². This has been beneficial in the quantification of plant substances³²⁻³⁴ and
32
33 deriving information regarding cell wall architecture³⁵⁻³⁸. FTIR has also contributed to our
34
35 understanding of key biotic and abiotic stresses such as plant-pathogen interactions and
36
37 salinity respectively^{28, 35, 39-41}. Furthermore, the imaging capabilities of FTIR spectroscopy,
38
39 particularly when utilised in conjunction with synchrotron radiation, have allowed the
40
41 development of high resolution chemical imaging for plant tissues including leaf⁴², seed^{43, 44}
42
43 and vascular tissues⁴⁵, that accurately portray biochemical distributions of the intrinsic
44
45 structure. However, the necessity of dried samples inhibits the use of FTIR for *in vivo* studies
46
47 and also results in substantial preparation time for *in situ* studies. This issue has in part been
48
49 overcome by the development of attenuated total reflection (ATR)-FTIR that utilises an
50
51 internal reflective element (IRE), commonly made of diamond, Ge or ZnSe, to produce an
52
53 evanescent wave that interrogates the sample in contact with the ATR attachment²⁸.
54
55
56
57
58
59
60

1
2
3
4
5
6
7
8
9
10
11
12
13
14
15
16
17
18
19
20
21
22
23
24
25
26
27
28
29
30
31
32
33
34
35
36
37
38
39
40
41
42
43
44
45
46
47
48
49
50
51
52
53
54
55
56
57
58
59
60

Consequently, analysis of fresh plant tissue *in situ* is possible and has so far been implemented in plant leaves to observe cell wall expansion⁴⁶, monitor temporal variations^{5, 47}, identify indicators of senescence⁴⁸, and also to characterise components of the epicuticular waxes^{49, 50}.

In comparison, Raman spectroscopy uses monochromatic light in the near-IR region in order to excite molecules to higher virtual energy states. The technique exploits the phenomena of inelastic, or Raman scattering, when a chemical bond is excited by an incidence ray to a virtual energy state but does not return to the original ground energy state, therefore resulting in an energy shift represented in spectra⁵¹. Although the occurrence of Raman scattering is a low probability process, the technique is highly sensitive with potential resolution approaching the nanometer scale⁵². Unlike IR spectroscopy, Raman spectroscopy is not inhibited by aqueous samples, as water molecules do not exhibit strong Raman scattering features, making the technique ideal for analysis of live material. However, progress in plant research has been impeded due to interference from autofluorescence of plant enzymes, which can completely suppress the Raman signal⁵³. The use of radiation in the near-IR (NIR) like that emitted from a Nd:YAG laser at 1064 nm, has been shown to reduce the influence of fluorescence on the Raman spectrum; however, this can also reduce spatial resolution and produce thermal emissions and absorption bands from hydrogen bonding^{54, 55}. Further development of the Raman technique has increased our ability to obtain stronger Raman signals free from autofluorescence. Surface-enhanced Raman scattering (SERS)^{35, 56, 57}, resonance Raman^{26, 58}, coherent anti-Stokes Raman scattering (CARS)^{59, 60}, and stimulated Raman scattering (SRS)³ have all contributed to improved resolution and the advancement of imaging capabilities in plant and crop science⁶¹. In particular, the use of metallic nanoparticles in SERS approaches have successfully quenched fluorescence that occurs in the

1
2
3 presence of chlorophyll and pheophytin, two key chromophores constituents of photosystems
4
5 situated on the thylakoid membrane of chloroplasts^{62, 63}.
6
7

8
9 IR spectroscopy is dependent on molecules being IR-active, therefore having a dipole
10
11 moment; however, Raman spectroscopy is reliant on molecules having polarisability. Thus in
12
13 combination the techniques are complementary and information that could be otherwise lost,
14
15 is regained by employing both techniques⁶⁴. Both systems are regarded as non-destructive
16
17 due to the use of relatively low energy lasers that are sufficient to vibrate but not damage
18
19 chemical bonds. In this study, ATR-FTIR and Raman spectroscopy are critically assessed as
20
21 analytical tools for non-destructive monitoring of plant health and development in *Solanum*
22
23 *lycopersicum* (tomato) leaves. An experimental overview can be seen in Figure 1. We
24
25
26 demonstrate that biochemical information regarding cell wall expansion during development
27
28 can be characterised *in vivo* without concerns from water and autofluorescence interference.
29
30
31
32
33
34
35

36 **Materials & Methods**

37 *Plant growth conditions*

38
39
40
41
42
43 *Solanum lycopersicum* cv. Moneymaker (Moles Seeds, Colchester, UK) were germinated and
44
45 cultivated individually in M3 compost (Levington Horticulture Ltd, Ipswich, UK) in a
46
47 controlled environment growth room and watered daily up to water-holding capacity.
48
49

50 Artificial light was generated by 600 W metal halide (Osram Ltd, UK) for 16 hour per day at
51
52 an intensity of $150 \pm 25 \mu\text{mol m}^{-2} \text{s}^{-1}$. The temperature was maintained at $25 \pm 2^\circ\text{C}$ and $20 \pm$
53
54 2°C for photophase and scotophase respectively. All plants were analysed in the middle of the
55
56 light period (12 - 4 pm) in order to maintain continuity. Prior and during spectral acquisition
57
58 in the lab, a portable light system was used to maintain optimum light levels.
59
60

Review of non-destructive analysis

Tomato plants ($t = 4$ weeks) were observed over a four week period in response to analysis by ATR-FTIR spectroscopy. Initially one set of plants ($n = 3$) was analysed by ATR-FTIR spectroscopy on a mature leaflet (A) for at least three time points across a seven day period. The following week another set of plants ($n = 3$) was introduced to the experiment, with all plants ($n = 6$) analysed on the same or equivalent leaflet three times across another seven day period. Additionally during this second week of analysis ($t = 5$ weeks) newly-expanded leaflets (B) from all plants in both sets were analysed to determine any systemic effects of the ATR-FTIR technique. This process was repeated for the following two weeks ($t = 6$ and 7 weeks), each time introducing a new set of previously unanalysed plants, comparing leaflets that had been previously analysed and newly expanded leaflets for systemic effects ($n = 12$, leaflets C and D respectively). Furthermore this methodology was repeated on separate tomato plants ($n = 9$) over a period of three weeks ($t = 4 - 6$ weeks) using Raman spectroscopy, to compare the destructive effects both locally and systemically on living tissue. A full overview of this process can be seen in the Electronic Supplementary Information (ESI) Figure S1. Simultaneously to all spectral acquisitions, measurements for rate of CO_2 assimilation, H_2O assimilation, internal CO_2 and stomatal conductance were obtained using a CIRAS-2 Portable Photosynthesis System (PP Systems, MA, USA) to determine any physiological indication of damage to the samples. Cuvette conditions corresponded to ambient CO_2 (390 ppm) light ($200 \mu\text{mol m}^{-2} \text{s}^{-1}$), temperature (22°C) and humidity (50 %) conditions within the controlled environment room.

Characterisation of healthy plant growth and development

Two time-course experiments over the course of three weeks were conducted in a total of nine tomato plants ($t = 4$ weeks), which were analysed using ATR-FTIR and Raman

1
2
3 spectroscopy at 12 and 11 different time points respectively. Three plants were analysed at
4
5 each time point to allow for sample rotation and high-throughput analysis. Each plant was
6
7 analysed on 3 separate leaves; a newly expanded (NE), a fully-expanded mature (M) and a
8
9 fully expanded senescing (S) leaf, to illustrate spectral alterations in leaves at distinct
10
11 morphological and developmental stages.
12
13

14 15 16 *ATR-FTIR spectroscopy*

17
18
19 IR spectra were derived using a Bruker TENSOR 27 FTIR spectrometer with Helios ATR
20
21 attachment (Bruker Optics, Coventry, UK). The approximate sampling area was 250 $\mu\text{m} \times$
22
23 250 μm as defined by the IRE, diamond crystal. Spectra were obtained at a spectral resolution
24
25 of 8 cm^{-1} , resulting in 3.84 cm^{-1} data spacing, with 32 co-additions and a mirror velocity of
26
27 2.2 kHz for optimum signal to noise ratio^{9, 28}. Five spectra were obtained from separate
28
29 locations on each sample leaf with the diamond crystal cleaned using distilled water and dried
30
31 between each measurement. Additionally, a background measurement was taken before each
32
33 new sample to account for any changes in atmospheric conditions. Whole plant samples were
34
35 positioned carefully around the spectrometer, with individual leaflets rested upon MirrIR
36
37 Low-E glass slides (Kevley Technologies, OH, USA) on the sample stage. Raw spectra were
38
39 cut at the spectral fingerprint region between 1800 - 900 cm^{-1} where biological molecules are
40
41 known to absorb, second order differentiated for baseline correction and vector normalised
42
43 using Matlab 2013a software (The Maths Works, MA, USA) with open-source IRootLab
44
45 graphical interface (<https://code.google.com/p/irootlab/>)^{65, 66}. The penetration depth (d_p) of
46
47 the ATR-FTIR evanescent wave varies between 0.5 - 2.9 μm at 4000 - 700 cm^{-1}
48
49 wavenumbers^{9, 47}. This infers that this technique can derive information predominantly from
50
51 the plant leaf cuticle (0.1 - 10 μm), the extracellular matrix of epidermal cells walls that is an
52
53 essential barrier for water loss and protection^{67, 68}.
54
55
56
57
58
59
60

Raman Spectroscopy

An InVia Renishaw Raman spectrometer with a 785 nm excitation laser (Renishaw Plc, Gloucestershire, UK), with charged couple detector (CCD) and microscope attachment (Leica Microsystems, Milton Keynes, UK) was employed to acquire Raman spectra. The system was calibrated using a silicon source prior to any sample analysis. Plants were positioned around the microscope stage and individual leaflets were rested upon gold-coated glass slides (Platypus Technologies, WI, USA). Ten spectra per sample were obtained at using a 1200 l/mm grating, $\times 50$ objective (0.75 numerical aperture), 50% laser power (13 mW at sample), 10 seconds exposure time and one accumulation within the spectral range 500 - 2000 cm^{-1} for optimum resolution ($\sim 1 \mu\text{m}$). The zap function in Renishaw Wire 3.1 software was used to remove any cosmic ray artefacts from spectra, and the IRootLab Matlab interface was employed to truncate spectra between 1750 - 700 cm^{-1} , baseline correct (1st order differentiation), vector normalise and wavelet de-noise⁶⁹. The d_p of Raman spectroscopy can be up to several hundred micrometres in living tissues, therefore spectral analysis of leaf tissue could interrogate both the cuticle and the underlying adaxial epidermal cells and potentially the palisade parenchyma⁷⁰. However in this investigation, focus is placed upon examination of the cuticle and epidermal cell wall.

Computational Analysis

Dataset analysis was conducted using the IRootLab toolbox for Matlab, unless otherwise stated. Spectral datasets are often complex, with each spectrum containing around 235 and up to 900 data points for ATR-FTIR and Raman spectra, respectively. Subsequently any underlying variance within these datasets can be difficult to unearth and feature extraction is essential⁷¹. Exploratory principal component analysis (PCA), following spectral standardisation, is an unsupervised technique that effectively reduces the dataset into

1
2
3 principal components (PCs), which encapsulate variance throughout data classes⁷². Coupled
4
5 with supervised linear discriminant analysis (LDA), a technique to attain inter-class
6
7 separation and minimize intra-class differences, a critical insight into spectral variance can be
8
9 ascertained⁷³. The number of PCs used was optimised using the PCA Pareto function within
10
11 the IRootLab toolbox, in order to prevent noise introduction, and K-fold, leave-one-out,
12
13 cross-validation was conducted to prevent over-fitting⁷¹.
14
15
16

17
18 For biomarker identification, three main approaches were conducted in order to visualise
19
20 developmental differences in leaves over time. Difference between mean spectra (DBM) is an
21
22 unsophisticated approach where mean spectra from two classes are subtracted, creating a
23
24 curve of fundamental wavenumber differences between them⁷⁴. The cluster vector (CV)
25
26 approach takes input from data reduction by PCA and consequent linear combination of
27
28 variables from LDA, to create a loadings vector for each class that passes through respective
29
30 data points⁷⁵. The pseudo-spectra that are created allow one to identify which variables, or
31
32 wavenumbers, are responsible for variance in the data set in direct relation to the original
33
34 absorbance/intensity spectrum⁷³. Forward feature selection (FFS) periodically incorporates
35
36 sub-sets of wavenumbers into a data set and ranks them based on their contribution to
37
38 improved classification, producing a feature selection histogram that visualises the number of
39
40 times each wavenumber was selected^{71, 74}. A Gaussian fit classifier was used with random
41
42 sub-sampling, repeated 100 times to randomise training and test data (90% training, 10%
43
44 data), and 10 variables were employed to improve stability of biomarker identification⁷⁶.
45
46 Wavenumbers were extracted using a peak detection algorithm as described by Coombes et
47
48 al. 2003⁷⁷. Following biomarker extraction, linear regression was conducted on mean
49
50 absorbance/intensity values between leaves at distinct developmental stages, to characterise
51
52 heterogeneity between leaves.
53
54
55
56
57
58
59
60

Potential anomalies were identified using the Grubb's test and one-way analysis of variance (ANOVA) with Tukey's multiple comparison tests were conducted in GraphPad Prism 4 software (GraphPad Software Inc, CA, USA) to determine significant differences between classes. Statistical tests were conducted using mean data from each sample, as opposed to individual scores.

Results and Discussion

Review of non-destructive analysis

In order to identify any destructive effects of either ATR-FTIR or Raman spectroscopy on living plant samples, a number of comparisons between leaflet observations were made. Initially, physical damage to the leaf was assessed visually to detect any signs of tissue damage and stress. Raman spectroscopy did not contribute to any visual alterations in leaf tissue viability in comparison to control leaves; however, ATR-FTIR spectroscopy resulted in clear indentation of the tissue (Fig. 2). This occurs as the technique requires contact between the diamond crystal and the sample, resulting in pressure being applied to the adaxial leaf surface and therefore causing damage to the cuticle and epidermis. Although local damage can be seen at the analysis site, no differences can be seen at other leaflets and systemic leaves, indicating that any damage is confined to the defined leaflet. Interestingly, no significant alterations can be observed when rates of CO₂ assimilation were compared between leaflet samples (Table 1) following interrogation by ATR-FTIR spectroscopy in both local and systemic leaves, despite compromises to the leaf surface. No significant alterations were apparent in additional gas exchanges measurements either (ESI Table S1). It can be assumed that there is no significant effect on CO₂ assimilation as a consequence of analysis using ATR-FTIR and therefore no apparent impact on leaf functionality.

1
2
3
4
5
6
7
8
9
10
11
12
13
14
15
16
17
18
19
20
21
22
23
24
25
26
27
28
29
30
31
32
33
34
35
36
37
38
39
40
41
42
43
44
45
46
47
48
49
50
51
52
53
54
55
56
57
58
59
60

Vibrational spectroscopy is a valuable tool for analysis of plant material and can infer subtle alterations in structure and biochemical composition that can be indicative of environmental stress^{5, 78}. Minimal variations can be seen in pre-processed mean spectra from both ATR-FTIR and Raman spectra (ESI Figs. S2 and S3) when comparing the effects of both analysis techniques in previously analysed and systemic leaves. This displays similarity in leaf stage of development, but also indicates the necessity of a feature extraction technique to identify subtle variation between samples that reveal biomarkers of damage. One-dimensional (1D) scores plots produced by cross-validated PCA-LDA of IR spectral data across the course of three weeks are shown (Fig. 3). Figure 3.A shows variance between equivalent leaflets at week 5 of plant development in two plant sets, one of which had been previously analysed using the ATR-FTIR technique. Spectra are plotted as points against the first linear discriminant (LD1), where separation in the y-axis suggests difference between the individual classes and consequently the samples. In this scores plot, initially no separation can be identified between 'plant set 1' and 'plant set 2' in either leaflet A (full square), which is a direct comparison between an interrogated leaflet and an equivalent non-interrogated leaflet. This suggests that there is no spectral alteration between the two that can be associated with continued analysis with ATR-FTIR spectroscopy, which is also confirmed by a one-way ANOVA test with Tukey's post-hoc test on each average sample score (ESI Table 2.A). Similarly in a systemic leaf, leaflet B in both plant sets, no differences can be seen showing that the technique is not causing any distinguishable damage to the overall plant health. Individual time points are identified using colour shading of individual spectra in order to identify any time related patterns; however, none are apparent.

During the following week of analysis (Fig. 3.B), small alterations can be observed between leaflet B in both 'plant set 2', which had been analysed since week 5 of development, and the newly introduced 'plant set 3'. This alteration may be due to the effect of the ATR-FTIR

1
2
3
4
5
6
7
8
9
10
11
12
13
14
15
16
17
18
19
20
21
22
23
24
25
26
27
28
29
30
31
32
33
34
35
36
37
38
39
40
41
42
43
44
45
46
47
48
49
50
51
52
53
54
55
56
57
58
59
60

technique on the integrity of the leaf. However, a degree of overlap occurs and following statistical analysis, this spectral feature is in fact not significant (ESI Table S2.B).

Interestingly, no statistically significant shifts in LD1 are present in leaflet C across all three plant sets, notwithstanding a potential outlier that could be associated with analysis at the beginning of the time period (ESI Table S2.C). In Figure 3.C, the final week of analysis is shown ($t = 7$) and a comparison between 'plant set 3' and 'plant set 4' in leaflet C indicates no movement in LD1, demonstrating no spectral effects due to previous analysis using ATR-FTIR spectroscopy. This is replicated in leaflet D across all four plant sets, which highlight the lack of systemic effects on overall plant health. Deterioration of leaf integrity would be identifiable via IR spectroscopy as key biochemical alterations occur during senescence including higher absorption at $1650 - 1500 \text{ cm}^{-1}$ corresponding to phenolic and proteinaceous compounds⁴⁸. Therefore any indication of leaf degradation or senescence induced by the technique would be observable using the multivariate method of analysis shown in Figure 3.

Following cross-validated PCA-LDA manipulation of Raman spectra, 1D scores plots comparing leaflets against LD1 display little separation or variance between data classes (Fig. 4). This observation corresponds with the lack of visual damage to the leaf surface, unlike the clear physical effects of the ATR-FTIR technique (Fig. 2). It is for this reason that analysis was conducted using the Raman across three weeks of development ($t = 4, 5$ and 6) as such minimal effects were perceived. Figure 4.A compares spectral differences between leaflet A in 'plant set 1', analysed during week 4 of plant development, and in 'plant set 2' newly introduced at week 5. The scores plot shows almost identical spectral responses between the equivalent leaflets, depicting heterogeneity between both classes (ESI Table S3). This pattern is also replicated in leaflet B, representing the systemic health of the plant away from the site of interrogation. Following an additional week of analysis, further alterations between leaflet B in 'plant sets 2' and '3' cannot be distinguished (Fig. 4.B). Furthermore, systemic effects

1
2
3 on plant health shown by comparison of leaflet C in 'plant sets 1', '2' and '3', indicate no
4 spectral separation in LD1 and therefore display no observable effect of interrogation using
5 Raman spectroscopy.
6
7
8
9

10 *Characterisation of healthy plant growth and development*

11
12
13 Establishment of both ATR-FTIR and Raman spectroscopy as entirely non-destructive, non-
14 invasive techniques with high throughput and resolution capabilities, indicates huge potential
15 in the research fields of plant science. Firstly, it is important to typify healthy plant growth
16 and identify key spectral biomarkers that are indicative of normal leaf development in an *in*
17 *vivo* system. Pre-processed FTIR spectra shown in Figure 5.A, depict well-defined time
18 dependent alterations across two distinct spectral regions: the polysaccharide fingerprint
19 region from 1000 - 1150 cm^{-1} ⁴¹ and the protein absorbance region between 1500 - 1700 cm^{-1}
20 wavenumbers⁴². Interestingly, there is an opposite response at each of these regions, with a
21 reduction in absorbance over time apparent at 1570, 1639 and 1709 cm^{-1} , associated with
22 protein absorbance and an increase observed at 1018, 1107 and 1125 cm^{-1} in the
23 polysaccharides region. During leaf development, it has been shown that plant cell walls
24 undergo secondary cell wall formation, mediated by expansin proteins that allow for
25 expansion of the cell wall by introduction of matrix polysaccharides such as cellulose, pectin
26 and hemi-celluloses⁷⁹. This correlates to the increased absorbance over time, with cellulose
27 alterations identified primarily at 1125 cm^{-1} ³², as well as 1107 and 1018 cm^{-1} with additional
28 contributions from pectin and hemicelluloses^{34, 80}. At the higher end of the spectrum, a
29 decrease in overall protein contribution can be seen at the amide I and amide II peaks, 1639
30 and 1570 cm^{-1} respectively, which could be tentatively associated with progression towards
31 leaf senescence during the analysis period⁴⁸. In comparison, class mean spectra obtained
32 using Raman spectroscopy do not reveal any obvious spectral differences due to growth and
33 development of the leaves (Fig. 5.B) and therefore further multivariate analysis is necessary
34
35
36
37
38
39
40
41
42
43
44
45
46
47
48
49
50
51
52
53
54
55
56
57
58
59
60

1
2
3 to distinguish biochemical features. It is important to note, that the Raman spectra derived
4 from *in vivo* analysis of plant samples has good signal to noise ratio and good spectral
5 resolution, despite potential issues surrounding autofluorescence. Any minimal effect of this
6 phenomenon has been alleviated or removed by baseline correction.
7
8
9

10
11
12
13 Cross-validated PCA-LDA with optimised PC factors was conducted on both FTIR
14 absorbance (Fig. 5.C) and Raman scattering (Fig. 5.D) spectra in order to elucidate variance
15 patterns within the data that correspond to the time progression. Figure 5.C shows a 1D
16 scores plot that illustrates a gradual migration in LD1, indicating an additive effect of subtle
17 spectral alterations between data classes. These differences are highly significant between
18 relatively equal time periods of around 7 days, effectively splitting the classes into two,
19 which potentially allows for grouping of different time points that would aid spectral analysis
20 by reducing class size (ESI Table S4). PCA-LDA of Raman spectra displays few significant
21 alterations between classes initially, indicating lack of change within the plant leaf samples
22 (Fig. 5.D). However, a clear shift is seen mid-way through the study shown in blue (day 9),
23 followed by a steady progression back to the starting baseline. This feature is likely to be
24 attributed to the spectral variation shown in Figure 5.B, which has increased absorbance
25 between 890 - 850 cm^{-1} , tentatively associated with cellulose⁶¹. The reason for this artefact
26 could be tentatively associated with secondary cell wall expansion, resulting in sampling at a
27 different region of the leaf tissue, from initially the epidermal cell layer itself, to the then
28 thickened cell wall.
29
30
31
32
33
34
35
36
37
38
39
40
41
42
43
44
45
46
47
48
49
50

51
52 As both data sets depict overlap between adjacent time points on 1D cross-validated PCA-
53 LDA scores plots, classes were merged to reduce number of classes and aid in visualisation
54 of spectral alterations. *P*-values relating to 1D scores plots, ATR-FTIR classes effectively
55 split the data set into two halves, which were then split again to produce four classes, each
56 ranging from 3-5 days of acquisition (ESI Table S4). This grouping was simulated in Raman
57
58
59
60

1
2
3 data, despite more varied significance patterns between classes. In doing so, the deviations in
4 protein and polysaccharide intensity seen previously in FTIR data are emphasised further and
5 optimised for biomarker extraction (Fig. 6.A and C). Although few differences were visible
6
7
8
9
10 in class means spectra of leaf samples using Raman spectroscopy, by grouping the individual
11 time point classes these subtle changes are accentuated and simplified (Fig. 8.B). Upon closer
12 inspection, it is possible to see a reduction in Raman scattering at 1233 cm^{-1} which is
13
14
15 conventionally associated with the amide III peak, mirroring the decline in protein content
16 and structure found in ATR-FTIR spectra⁵⁵. Furthermore, a decline in chlorophyll content is
17
18
19 observed at 1534 cm^{-1} representing a well-characterised indication of senescence as
20
21
22 chloroplasts are degenerated^{81,82}. This is a particularly good example of the complementary
23 nature of both the ATR-FTIR and Raman techniques. Additional spectral differences are
24
25
26 visible in the Raman polysaccharide region, between $1160 - 970\text{ cm}^{-1}$ associated
27
28
29 predominantly with cellulose⁵⁵. At this stage no overall change in cellulose can be identified;
30
31
32 conflicting intensity patterns at 1054 cm^{-1} , which displays a reduction over time, and 1139
33
34
35 cm^{-1} that depicts an increase over time, provide unclear evidence for cellulose alterations. By
36
37
38 grouping together equivalent classes, 1D scores plots following PCA-LDA show that group
39
40
41 'Days 8 - 11' significantly deviates from the other data classes (Fig. 6.D).
42

43
44 A number of feature extraction methods are available to feed into biomarker determination
45 and classification models⁷¹. In this study, three approaches are explored to ascertain robust
46
47
48 biomarkers suggestive of standard leaf development: DBM (top panels, \circ), CV approach
49
50
51 (middle panel, \square) and FFS histograms (bottom panels, Δ). In each instance, the first data
52
53
54 group 'Days 1 - 3' was used as a reference class and any consequent changes along the
55
56
57 biological spectrum would be indicative of developmental alterations from this starting point
58
59
60 of spectral acquisition. The top six biomarkers for each approach were identified using a peak
detection algorithm and are listed in Table 2.

1
2
3 Initially, by comparing 'Days 1 - 3' with 'Days 4 - 7' from ATR-FTIR analysis it is clear to
4 see a number of potential wavenumbers emerging from all three feature extraction methods
5
6 (Fig. 7.A). The DBM approach identifies wavenumbers principally from the protein and
7
8 polysaccharide regions, emulating patterns identified in class means spectra. This is also
9
10 replicated in CV and FFS analysis, additional to a number of wavenumbers across the
11
12 spectrum that are also classified. Table 3 describes the top three biomarkers from each
13
14 comparison, derived from wavenumbers uncovered by two or more biomarker extraction
15
16 approaches, with a tentative band assignment. As shown previously, the main alterations in
17
18 Figure 7. A are found at 1107 and 1408 cm^{-1} accounting for pectin found in the plant cell
19
20 wall, as well as at $\sim 1510 \text{ cm}^{-1}$, tentatively assigned to lignin or protein⁸⁰. Lignin is present in
21
22 vascular bundles within a tomato leaf and so may be noticeable due to spectral acquisition on
23
24 the leaf midrib or because of damage to the leaf surface during analysis. When comparing
25
26 'Days 1 - 3' with 'Days 8 - 11' alterations in the protein regions manifests across all three
27
28 approaches with the amide III peak at 1302 cm^{-1} being the most discriminating (Fig. 7.B).
29
30 The DBM and CV methodology also show similarities in polysaccharide alterations,
31
32 particularly at 1103 cm^{-1} associated with ester and pectins, although this is not selected by the
33
34 FFS histogram. Ester bonds crosslink cutin in the leaf cuticle and thus this peak infers
35
36 information about this upper leaf surface layer⁸³. Figure 7.C illustrates parity between the
37
38 DBM, CV and FFS extraction methods with each approach consistently identifying protein
39
40 alterations at 1642 cm^{-1} the amide I peak, and carbohydrate markers at 1101 and 1014 cm^{-1}
41
42 assigned to cellulose and pectin respectively. As this is a comparison between the two
43
44 extreme time classes, the differences are expected to be more identifiable by all approaches.
45
46 Raman data compared between 'Days 1 - 3' and 'Days 4 - 7' show very little variation,
47
48 indicated by relatively noisy curves in both DBM and CV analysis and a featureless FFS
49
50 histogram (Fig. 7.D). As shown in ATR-FTIR data, these two data classes are most similar
51
52
53
54
55
56
57
58
59
60

1
2
3 and therefore spectral differences would be minimal. In contrast, Figure 7.E consistently
4
5 locates three distinct wavenumbers associated principally with carotenoid at 1158 and 1527
6
7 cm^{-1} , as well as chlorophyll at 1328 cm^{-1} . The latter of these observations may be expected as
8
9 a leaf develops towards senescence, due to a breakdown of chloroplasts and therefore a
10
11 decrease in chlorophyll content⁸⁴. The same wavenumbers are again deduced when
12
13 comparing 'Days 1 - 3' with 'Days 12 - 17', although surprisingly these are not picked out as
14
15 robustly in the FFS histogram (Fig. 7.F). Alterations at the 1158 and 1526 cm^{-1} band begins
16
17 to infer that there is a variance in carotenoid content between classes, attributed to leaf
18
19 development. It is well established that carotenoid content remains constant whilst
20
21 chlorophyll reduces through development of the leaf, evidenced by colour transition from
22
23 green to brown in young and senescent leaves⁸⁵. Thus any alteration in carotenoids pigments
24
25 is unexpected in regards to development of the leaf.
26
27
28
29
30
31

32
33 Linear regression analysis was conducted on the most distinguishing biomarkers previously
34
35 determined, to ascertain any patterns in absorbance between leaves at different morphological
36
37 stages (Fig. 8). In general, a negative relationship can be seen between protein absorbance
38
39 over time, particularly NE leaves, typified by IR absorbance values at 1639 cm^{-1} , representing
40
41 progression from young towards senescent leaf (Fig. 8.A). This is also replicated to a lesser
42
43 extent in M leaves, which is attributed to the leaf being closer to senescence and therefore not
44
45 experiencing as severe protein reduction in the acquisition time frame. No significant
46
47 decrease in protein can be identified in S leaves over the course of the study due to already
48
49 having undergone substantial protein degradation (ESI Table S5). Figure 8.B and C highlight
50
51 positive variations in absorbance bands at 1107 and 1015 cm^{-1} corresponding to
52
53 polysaccharides cellulose and pectin, respectively. NE leaves again depict the greatest
54
55 alterations at these wavenumbers corresponding to cell wall expansion. This pattern is less
56
57 visible in M leaves and even less so in S leaves, mirroring the response shown in protein. A
58
59
60

1
2
3
4
5
6
7
8
9
10
11
12
13
14
15
16
17
18
19
20
21
22
23
24
25
26
27
28
29
30
31
32
33
34
35
36
37
38
39
40
41
42
43
44
45
46
47
48
49
50
51
52
53
54
55
56
57
58
59
60

diminution of protein and increase of carbohydrate are simple characteristics of leaf development and have been effectively characterised here by ATR-FTIR in different leaf stages.

Figure 8.D shows linear regression analysis of scattering intensity at 1529 cm^{-1} resultant from Raman analysis of NE, M and S leaves. Although only minimal significance can be seen in M leaves, there is a slight negative trend in the data, showing a reduction in chlorophyll and carotenoid intensity. This acknowledged indicator of leaf senescence appears to occur more significantly in M leaves, highlighting that chlorophyll degradation in this case appears to be a late on-set process within leaf senescence⁸⁶. In contrast, at peak 1328 cm^{-1} corresponding primarily with chlorophyll, no significant patterns can be identified with NE expanded leaves showing slight increases compared with small reductions in M and S leaves (Fig. 8.E).

Overlap with DNA and protein can be observed around this region and may contribute to masking any chlorophyll scattering effect⁸⁷. Carotenoid alterations are portrayed in Figure 8.F relative to intensity at 1158 cm^{-1} and do not show any significant differences between leaf samples.

Conclusion

ATR-FTIR and Raman spectroscopy are highly informative, non-destructive and robust techniques that have been limitedly employed in the field of plant science³². Whilst many studies demonstrate the successful use of vibrational spectroscopy to characterise plant tissues in fixed and *in vitro* samples, thus far research has been hindered by water interference and auto-fluorescence³. In this investigation, *in vivo* spectral measurements are obtained with no destructive effect on systemic plant health. Although ATR-FTIR appears to cause minor local damage, this had no significant effect on the leaf and therefore does not necessarily rule out non-destructive analysis. The technique may not be suitable for direct

1
2
3 analysis of fruit or yieldable products, however in future field studies, a single leaf is more
4 easily sacrificed in a plant or crop system, with no detriment to crop yield or quality. Raman
5 spectroscopy in particular had little visible effect on plant health and viability and may prove
6 to be a crucial tool for live plant analysis. Additionally, both complementary methods
7 coupled with multivariate analysis, provide data that can accurately depict known plant
8 developmental processes, providing groundwork for characterisation of complex stress
9 responses, such as nutrient deficiency, that could be used in the field. A prerequisite for
10 future studies would be to characterise a stress response and locate spectral biomarkers
11 indicative of this given stress. This presents a novel method of fingerprinting plant health in a
12 high-throughput manner, which can be effectively employed in agricultural and
13 environmental studies.
14
15
16
17
18
19
20
21
22
23
24
25
26
27
28
29
30
31
32

33 **Acknowledgements**

34
35
36 HJB is a member of the Centre for Global Eco-Innovation with ERDF funding.
37
38
39
40
41
42
43
44
45
46
47
48
49
50
51
52
53
54
55
56
57
58
59
60

References

1. H. C. J. Godfray, J. R. Beddington, I. R. Crute, L. Haddad, D. Lawrence, J. F. Muir, J. Pretty, S. Robinson, S. M. Thomas and C. Toulmin, *Science*, 2010, **327**(5967): 812-818.
2. I. Domínguez-Martínez, O. G. Meza-Márquez, G. Osorio-Revilla, J. Proal-Nájera and T. Gallardo-Velázquez, *J. Korean Soc. Appl. Biol. Chem.*, 2014, **57**(1): 133-142.
3. J. C. Mansfield, G. R. Littlejohn, M. P. Seymour, R. J. Lind, S. Perfect and J. Moger, *Anal. Chem.*, 2013, **85**(10): 5055-5063.
4. V. Llabjani, R. N. Malik, J. Trevisan, V. Hoti, J. Ukpebor, Z. K. Shinwari, C. Moeckel, K. C. Jones, R. F. Shore and F. L. Martin, *Environ. Int.*, 2012, **48**: 39-46.
5. B. E. Obinaju, A. Alaoma and F. L. Martin, *Environ. Pollut.*, 2014, **192**: 222-231.
6. M. Mecozzi, M. Pietroletti and R. Di Mento, *Vib. Spectrosc.*, 2007, **44**(2): 228-235.
7. L. G. Thygesen, M. M. Løkke, E. Micklander and S. B. Engelsens, *Trends Food Sci. Tech.*, 2003, **14**(1): 50-57.
8. D.-W. Sun, *Infrared spectroscopy for food quality analysis and control*, Academic Press, 2009.
9. M. J. Baker, J. Trevisan, P. Bassan, R. Bhargava, H. J. Butler, K. M. Dorling, P. R. Fielden, S. W. Fogarty, N. J. Fullwood, K. A. Heys, C. Hughes, P. Lasch, P.L. Martin-Hirsch, B. Obinaju, G. D. Sockalingum, J. Sulé-Suso, R. J. Strong, M. J. Walsh, B. R. Wood, P. Gardner and F. L. Martin, *Nat. Protoc.*, 2014, **9**(8): 1771-1791.
10. J. M. Chalmers, P. R. Griffiths, D. E. Pivonka, J. Chalmers and P. Griffiths, *Applications of vibrational spectroscopy in pharmaceutical research and development*, Edited by: Pivonka, DE, Chalmers, JM and Griffiths, PR, 2007.

- 1
2
3
4 11. G. Clemens, J. R. Hands, K. M. Dorling and M. J. Baker, *Analyst*, 2014, **139**(18):
5
6 4411-4444.
- 7
8 12. P. Lasch, A. Pacifico and M. Diem, *Biopolymers*, 2002, **67**(4-5): 335-338.
- 9
10 13. M. Diem, A. Mazur, K. Lenau, J. Schubert, J. Fore, B. Bird, M. Miljković and C.
11
12 Krafft, in *Ex-vivo and In-vivo Optical Molecular Pathology*, ed. J. Popp, 2014, ch. 3,
13
14 pp. 45-102.
- 15
16 14. F. M. Lyng, E. Ó. Faoláin, J. Conroy, A. D. Meade, P. Knief, B. Duffy, M. Hunter, J.
17
18 Byrne, P. Kelehan and H. J. Byrne, *Exp. Mol. Pathol.*, 2007, **82**(2): 121-129.
- 19
20 15. D. C. Fernandez, R. Bhargava, S. M. Hewitt and I. W. Levin, *Nat. Biotechnol.*, 2005,
21
22 **23**(4): 469-474.
- 23
24 16. B. R. Wood, M. A. Quinn, F. R. Burden and D. McNaughton, *Biospectroscopy*, 1996,
25
26 **2**(3): 143-153.
- 27
28 17. P. Crow, A. Molckovsky, N. Stone, J. Uff, B. Wilson and L. Wongkeesong, *Urology*,
29
30 2005, **65**(6): 1126-1130.
- 31
32 18. N. Stone and P. Matousek, *Cancer Res.*, 2008, **68**(11): 4424-4430.
- 33
34 19. P. Lasch, W. Haensch, D. Naumann and M. Diem, *BBA-Molecular Basis of Disease*,
35
36 2004, **1688**(2): 176-186.
- 37
38 20. M. K. Kuimova, K. Chan and S. G. Kazarian, *Appl. Spectrosc.*, 2009, **63**(2): 164-171.
- 39
40 21. J. Ollesch, M. Heinze, H. M. Heise, T. Behrens, T. Brüning and K. Gerwert, *J.*
41
42 *Biophotonics*, 2014, **7**(3-4): 210-221.
- 43
44 22. K. M. Dorling and M. J. Baker, *Trends Biotechnol.*, 2013, **31**(6): 327-328.
- 45
46 23. D. Lin, S. Feng, J. Pan, Y. Chen, J. Lin, G. Chen, S. Xie, H. Zeng and R. Chen, *Opt.*
47
48 *Express*, 2011, **19**(14): 13565-13577.
- 49
50 24. J. W. Allwood, J. Heald, A. J. Lloyd, R. Goodacre and L. A. Mur, in *Plant*
51
52 *Metabolomics*, Springer, 2012, vol. 860, pp. 31-49.
- 53
54
55
56
57
58
59
60

- 1
2
3
4
5
6
7
8
9
10
11
12
13
14
15
16
17
18
19
20
21
22
23
24
25
26
27
28
29
30
31
32
33
34
35
36
37
38
39
40
41
42
43
44
45
46
47
48
49
50
51
52
53
54
55
56
57
58
59
60
25. M. Baranska, W. Schütze and H. Schulz, *Anal. Chem.*, 2006, **78**(24): 8456-8461.
26. D. Gill, R. Kilponen and L. Rimai, *Nature*, 1970, **227**(5259): 743-744.
27. R. H. Wilson, A. C. Smith, M. Kačuráková, P. K. Saunders, N. Wellner and K. W. Waldron, *Plant Physiol.*, 2000, **124**(1): 397-406.
28. H. E. Johnson, D. Broadhurst, R. Goodacre and A. R. Smith, *Phytochemistry*, 2003, **62**(6): 919-928.
29. Z. Wei, L. Dong and Z. Tian, *Pakistan J. Bot.*, 2009, **41**(4): 1743-1750.
30. P. Griffiths and J. A. De Haseth, *Fourier transform infrared spectrometry*, Wiley-Interscience, 2007.
31. F. L. Martin, *Nat. Methods*, 2011, **8**(5): 385-387.
32. H. Schulz and M. Baranska, *Vib. Spectrosc.*, 2007, **43**(1): 13-25.
33. Y. Li, D. Kong and H. Wu, *Ind. Crop. Prod.*, 2013, **41**(1): 269-278.
34. M. Kacurakova, P. Capek, V. Sasinkova, N. Wellner and A. Ebringerova, *Carbohydr. Polymers*, 2000, **43**(2): 195-203.
35. P. Rösch, W. Kiefer and J. Popp, *Biopolymers*, 2002, **67**(4-5): 358-361.
36. M. C. McCann, M. Defernez, B. R. Urbanowicz, J. C. Tewari, T. Langewisch, A. Olek, B. Wells, R. H. Wilson and N. C. Carpita, *Plant Physiol.*, 2007, **143**(3): 1314-1326.
37. M. McCann, L. Chen, K. Roberts, E. Kemsley, C. Sene, N. Carpita, N. Stacey and R. Wilson, *Physiol. Plant.*, 1997, **100**(3): 729-738.
38. D. Harris, V. Bulone, S.-Y. Ding and S. DeBolt, *Plant Physiol.*, 2010, **153**(2): 420-426.
39. R. Gessner, P. Rösch, R. Petry, M. Schmitt, M. Strehle, W. Kiefer and J. Popp, *Analyst*, 2004, **129**(12): 1193-1199.

- 1
2
3
4
5
6
7
8
9
10
11
12
13
14
15
16
17
18
19
20
21
22
23
24
25
26
27
28
29
30
31
32
33
34
35
36
37
38
39
40
41
42
43
44
45
46
47
48
49
50
51
52
53
54
55
56
57
58
59
60
40. E. Gidman, R. Goodacre, B. Emmett, A. R. Smith and D. Gwynn-Jones, *Phytochemistry*, 2003, **63**(6): 705-710.
41. J. W. Allwood, D. I. Ellis and R. Goodacre, *Physiol. Plant.*, 2008, **132**(2): 117-135.
42. P. Heraud, S. Caine, G. Sanson, R. Gleadow, B. R. Wood and D. McNaughton, *New Phytol.*, 2007, **173**(1): 216-225.
43. P. Yu, J. J. McKinnon, C. R. Christensen, D. A. Christensen, N. S. Marinkovic and L. M. Miller, *J. Agri. Food Chem.*, 2003, **51**(20): 6062-6067.
44. B. O. Budevskaja, S. T. Sum and T. J. Jones, *Appl. Spectrosc.*, 2003, **57**(2): 124-131.
45. D. S. Himmelsbach, S. Khalili and D. E. Akin, *J. Sci. Food Agr.*, 2002, **82**(7): 685-696.
46. F. Monti, R. Dell'Anna, A. Sanson, M. Fasoli, M. Pezzotti and S. Zenoni, *Vib. Spectrosc.*, 2012, **65**: 36-43.
47. B. Ribeiro da Luz, *New Phytol.*, 2006, **172**(2): 305-318.
48. D. G. Ivanova and B. R. Singh, *Biopolymers*, 2003, **72**(2): 79-85.
49. E. Dubis, A. Dubis and J. Morzycki, *J. Mol. Struct.*, 1999, **511**: 173-179.
50. E. N. Dubis, A. T. Dubis and J. Popławski, *J. Mol. Struct.*, 2001, **596**(1): 83-88.
51. E. B. Wilson, *Molecular vibrations: the theory of infrared and Raman vibrational spectra*, Courier Dover Publications, 1955.
52. E. Smith and G. Dent, *Modern Raman spectroscopy: a practical approach*, John Wiley & Sons, 2005.
53. M. Baranska, M. Roman, H. Schulz and R. Baranski, *Curr. Anal. Chem.*, 2013, **9**(1): 108-127.
54. B. Schrader, A. Hoffmann and S. Keller, *Spectrochim. Acta A - Molecular Spectroscopy*, 1991, **47**(9): 1135-1148.

- 1
2
3
4
5
6
7
8
9
10
11
12
13
14
15
16
17
18
19
20
21
22
23
24
25
26
27
28
29
30
31
32
33
34
35
36
37
38
39
40
41
42
43
44
45
46
47
48
49
50
51
52
53
54
55
56
57
58
59
60
55. C. Sene, M. C. McCann, R. H. Wilson and R. Grinter, *Plant Physiol.*, 1994, **106**(4): 1623-1631.
56. L. Zeiri, *J. Raman Spectrosc.*, 2007, **38**(7): 950-955.
57. P. Rösch, J. Popp and W. Kiefer, *J. Mol. Struct.*, 1999, **480–481**: 121-124.
58. J. C. Merlin, *Pure Appl. Chem.*, 1985, **57**(5): 785-792.
59. Y. Zeng, M. E. Himmel and S.-Y. Ding, in *Biomass Conversion*, Springer, Methods in Molecular Biology, 2012, vol. 908, pp. 49-60.
60. Y. Zeng, B. G. Saar, M. G. Friedrich, F. Chen, Y.-S. Liu, R. A. Dixon, M. E. Himmel, X. S. Xie and S.-Y. Ding, *Bioenerg. Res.*, 2010, **3**(3): 272-277.
61. M. Chylinska, M. Szymanska-Chargot and A. Zdunek, *Plant Methods*, 2014, **10**(1): 14.
62. R. Picorel, G. Chumanov, E. Torrado, T. M. Cotton and M. Seibert, *J. Phys. Chem. B*, 1998, **102**(15): 2609-2613.
63. M. Seibert, R. Picorel, J.-H. Kim and T. M. Cotton, *Method. Enzymology*, 1992, **213**: 31-42.
64. B. Schrader, *Infrared and Raman spectroscopy: methods and applications*, John Wiley & Sons, 2008.
65. F. L. Martin, J. G. Kelly, V. Llabjani, P. L. Martin-Hirsch, I. I. Patel, J. Trevisan, N. J. Fullwood and M. J. Walsh, *Nat. Protoc.*, 2010, **5**(11): 1748-1760.
66. J. Trevisan, P. P. Angelov, A. D. Scott, P. L. Carmichael and F. L. Martin, *Bioinformatics*, 2013, **29**(8): 1095-1097.
67. E. Domínguez, J. A. Heredia-Guerrero and A. Heredia, *New Phytol.*, 2011, **189**(4): 938-949.
68. M. Riederer and L. Schreiber, *J. Exp. Bot.*, 2001, **52**(363): 2023-2032.
69. G. Strang and T. Nguyen, *Wavelets and filter banks*, SIAM, 1996.

- 1
2
3
4
5
6
7
8
9
10
11
12
13
14
15
16
17
18
19
20
21
22
23
24
25
26
27
28
29
30
31
32
33
34
35
36
37
38
39
40
41
42
43
44
45
46
47
48
49
50
51
52
53
54
55
56
57
58
59
60
70. P. Matousek, *Chem. Soc. Rev.*, 2007, **36**(8): 1292-1304.
71. J. Trevisan, P. P. Angelov, P. L. Carmichael, A. D. Scott and F. L. Martin, *Analyst*, 2012, **137**(14): 3202-3215.
72. Patel, II, W. J. Harrison, J. G. Kerns, J. Filik, K. Wehbe, P. L. Carmichael, A. D. Scott, M. P. Philpott, M. D. Frogley, G. Cinque and F. L. Martin, *Anal. Bioanal. Chem.*, 2012, **404**(6-7): 1745-1758.
73. F. L. Martin, M. J. German, E. Wit, T. Fearn, N. Ragavan and H. M. Pollock, *J. Comp. Biol.*, 2007, **14**(9): 1176-1184.
74. J. Trevisan, P. P. Angelov, I. I. Patel, G. M. Najand, K. T. Cheung, V. Llabjani, H. M. Pollock, S. W. Bruce, K. Pant and P. L. Carmichael, *Analyst*, 2010, **135**(12): 3266-3272.
75. J. G. Kelly, J. I. Trevisan, A. D. Scott, P. L. Carmichael, H. M. Pollock, P. L. Martin-Hirsch and F. L. Martin, *J. Prot. Res.*, 2011, **10**(4): 1437-1448.
76. J. Trevisan, J. Park, P. P. Angelov, A. A. Ahmadzai, K. Gajjar, A. D. Scott, P. L. Carmichael and F. L. Martin, *J. Biophotonics*, 2014, **7**(3-4): 254-265.
77. K. R. Coombes, H. A. Fritsche, C. Clarke, J.-N. Chen, K. A. Baggerly, J. S. Morris, L.-C. Xiao, M.-C. Hung and H. M. Kuerer, *Clin. Chem.*, 2003, **49**(10): 1615-1623.
78. I. Weissflog, N. Vogler, D. Akimov, A. Dellith, D. Schachtschabel, A. Svatos, W. Boland, B. Dietzek and J. Popp, *Plant Physiol.*, 2010, **154**(2): 604-610.
79. D. J. Cosgrove, *Nat. Rev. Mol. Cell Biol.*, 2005, **6**(11): 850-861.
80. Z. Movasaghi, S. Rehman and D. I. ur Rehman, *Appl. Spectrosc. Rev.*, 2008, **43**(2): 134-179.
81. C. M. Smart, *New Phytol.*, 1994, **126**(3): 419-448.
82. V. Buchanan-Wollaston, *J. Exp. Bot.*, 1997, **48**(2): 181-199.

- 1
2
3
4
5
6
7
8
9
10
11
12
13
14
15
16
17
18
19
20
21
22
23
24
25
26
27
28
29
30
31
32
33
34
35
36
37
38
39
40
41
42
43
44
45
46
47
48
49
50
51
52
53
54
55
56
57
58
59
60
83. P. Kolattukudy, K. Espelie and C. Soliday, in *Plant Carbohydrates II*, Springer, 1981, pp. 225-254.
84. B. Schrader, B. Dippel, I. Erb, S. Keller, T. Löchte, H. Schulz, E. Tatsch and S. Wessel, *J. Mol. Struct.*, 1999, **480–481**(0): 21-32.
85. R. Baranski, M. Baranska and H. Schulz, *Planta*, 2005, **222**(3): 448-457.
86. L. Guyer, S. S. Hofstetter, B. Christ, B. S. Lira, M. Rossi and S. Hörtensteiner, *Plant Physiol.*, 2014, **166**(1): 44-56.
87. Z. Movasaghi, S. Rehman and I. U. Rehman, *Appl. Spectrosc. Rev.*, 2007, **42**(5): 493-541.
88. L. Chen, N. C. Carpita, W.-D. Reiter, R. H. Wilson, C. Jeffries and M. C. McCann, *Plant J.*, 1998, **16**(3): 385-392.
89. R. Hunt, *Basic growth analysis*, Unwin Hyman Ltd, 1990.
90. H. Schulz, M. Baranska and R. Baranski, *Biopolymers*, 2005, **77**(4): 212-221.
91. J. J. Jansen, J. W. Allwood, E. Marsden-Edwards, W. H. van der Putten, R. Goodacre and N. M. van Dam, *Metabolomics*, 2009, **5**(1): 150-161.

Legends to figures

Figure 1. An overview of the experimental principles and procedure. ATR-FTIR and Raman spectroscopy rely on distinctly different physical processes and therefore have discrete targets in the leaf tissue, with the cuticle being interrogated by both techniques and the epidermis and palisade parenchyma by Raman alone.

Figure 2. Visible effect of ATR-FTIR spectroscopy on leaf tissue. (A) depicts leaflet sample immediately following analysis at three distinct points ($t = 4$ weeks) and (B) shows the same leaflet one week later ($t = 5$ weeks).

Figure 3. Cross-validated PCA-LDA 1D scores plot of ATR-FTIR spectra obtained over a three week period ($t =$ weeks 5, 6 and 7 of development) to distinguish spectral effects of the technique. Each square corresponds to an individual spectrum, and colour variation indicates advancing time points through the respective time frame. Full squares (■) represent a comparison between leaflets specifically analysed the previous week with equivalent leaflets from a newly introduced plant set, and empty squares (□) compare a newly expanded leaflet to observe any systemic effects as well as local effects of the technique. (A) Compares previously analysed leaflet A and systemic leaflet B in plant sets 1 and 2; (B) leaflets B and C and (C) leaflets C and D.

Figure 4. Cross-validated PCA-LDA 1D scores plot of Raman spectra obtained over a two week period ($t =$ weeks 5 and 6 of development) to distinguish spectral effects of the technique. Each point corresponds to an individual spectrum, and colour variation indicates advancing time points through the respective time frame. Full circles (●) represent a comparison between leaflets specifically analysed the previous week with equivalent leaflets from a newly introduced plant set, and empty circles (○) compare a newly expanded leaflet to

1
2
3 observe any systemic and local effects of the technique. (A) Compares previously analysed
4 leaflet A and systemic leaflet B in plant sets 1 and 2 and (B) leaflets B and C.
5
6
7

8
9 **Figure 5.** Spectral data derived from ATR-FTIR (A and C) and Raman (B and D)
10 spectroscopy over time points spanning a three week period in order to identify alterations
11 indicative of healthy growth. (A) ATR-FTIR class means spectra of pre-processed data, cut to
12 1800 - 900 cm^{-1} wavenumbers, 2nd order differentiation baseline correction and vector
13 normalisation; (B) Raman class means spectra cut to 1750 - 700 cm^{-1} wavenumbers, 1st order
14 differentiated, vector normalised and wavelet de-noised; (C) cross-validated PCA-LDA 1D
15 scores plot of ATR-FTIR spectra in regards to LD1 (D) cross-validated PCA-LDA 1D scores
16 plot of Raman spectra across LD1.
17
18
19
20
21
22
23
24
25
26
27

28
29 **Figure 6** Spectra derived from ATR-FTIR (A and C) and Raman (B and D) spectroscopy
30 with grouped time points in order to depict clear spectral differences symptomatic of leaf
31 development. (A) ATR-FTIR pre-processed class means spectra, cut to 1800 - 900 cm^{-1} , 2nd
32 order differentiation and vector normalised; (B) Raman class means spectra cut to 1750 - 700
33 cm^{-1} , 1st order differentiation base line correction, vector normalised and wavelet de-noised;
34 (C) cross-validated PCA-LDA 1D scores plot of ATR-FTIR spectra against LD and (D)
35 cross-validated PCA-LDA scores plot of Raman spectra across LD1.
36
37
38
39
40
41
42
43
44
45

46
47 **Figure 7.** Three biomarker extraction approaches, difference between mean spectra (top
48 panels), PCA-LDA cluster vector (middle panels) and forward feature selection histograms
49 (bottom panels) to establish spectral biomarkers indicative of plant development in both
50 ATR-FTIR and Raman data. 'Days 1 - 3' represent the initial spectral characterisation of the
51 leaf and therefore 'Days 4 - 7' (A and D); 'Days 8 - 11' (B and E); and 'Days 12 - 17' (C and
52 F) are all compared to this data class. The top six biomarkers identified in each approach are
53 highlighted with symbols. All units are arbitrary.
54
55
56
57
58
59
60

1
2
3
4 **Figure 8.** Linear regression analysis at key biomarker wavenumbers 1639 cm⁻¹ (A), 1103 cm⁻¹ (B), 1015 cm⁻¹ (C) from mean IR spectra and 1529 cm⁻¹ (D), 1327 cm⁻¹ (E), 1158 cm⁻¹ (F)
5
6
7
8 from mean Raman spectra of leaves at different developmental stages.
9
10
11
12
13
14
15
16
17
18
19
20
21
22
23
24
25
26
27
28
29
30
31
32
33
34
35
36
37
38
39
40
41
42
43
44
45
46
47
48
49
50
51
52
53
54
55
56
57
58
59
60

1
2
3
4
5
6
7
8
9
10
11
12
13
14
15
16
17
18
19
20
21
22
23
24
25
26
27
28
29
30
31
32
33
34
35
36
37
38
39
40
41
42
43
44
45
46
47
48
49
50
51
52
53
54
55
56
57
58
59
60

Tables

Table 1. Average rate of CO₂ assimilation ($\mu\text{mol CO}_2 \text{ m}^{-2} \text{ s}^{-1} \pm$ standard error) for equivalent leaflets (A-D) in four plant sets over a time course of three weeks ($t = 5-7$) to determine any detrimental effects of ATR-FTIR spectroscopy interrogation. An ANOVA test was performed to determine any significant differences between values, however no significance was depicted ($P > 0.05$). Leaflets previously analysed using the technique are shown in italic.

Leaflet	<i>t = 5 weeks</i>		<i>t = 6 weeks</i>		<i>t = 7 weeks</i>	
	A	B	B	C	C	D
1	<i>8.03 ± 0.61</i>	<i>10.54 ± 0.99</i>	–	<i>11.39 ± 1.72</i>	–	<i>10.65 ± 0.44</i>
2	<i>6.44 ± 0.40</i>	<i>12.26 ± 0.59</i>	<i>6.97 ± 0.97</i>	<i>12.70 ± 1.22</i>	–	<i>11.86 ± 0.79</i>
3			<i>8.66 ± 1.59</i>	<i>10.36 ± 1.73</i>	<i>12.28 ± 1.84</i>	<i>10.63 ± 1.49</i>
4					<i>6.70 ± 1.78</i>	<i>6.82 ± 1.25</i>

Table 2. Key wavenumber features determined by difference between mean (DBM), cluster vector (CV) and forward feature selection (FFS) biomarker extraction methods, as identified in Figure 9. Wavenumbers are displayed in descending order of significance and bold type represents wavenumbers identified in two or more extraction methods.

Top six discriminating biomarkers (cm ⁻¹)				
	Classes	DBM	CV	FFS
ATR -FTIR	Days 1-3 versus Days 4-7	1107*	968	1192
		1547	1057	1408
		1643	1705	1327
		1018	1408	1508
		1126	1254	1076
		1593	1512	1666
	Days 1-3 versus Days 8-11	1103*	1331	1408
		1639	968	1508
		1018	1057	1470
		1126	1466	1358
		1547	1308	1296
		1593	1254	1666
	Days 1-3 versus Days 12-17	1639	1327	1647
		1015	1636	1751
		1103	1308	1574
		1123	1466	1431
		991	1597	1099
		1038	1011	990
Raman	Days 1-3 versus Days 4-7	704	1318	1464
		723	1173	1191
		1229	1130	1654
		1173	1217	1321
		1103	1423	911
		1513	718	1628
	Days 1-3 versus Days 8-11	1158	1328	1527
		1327	1157	1328
		1526	1526	1157
		1513	1287	1689
		744	1186	1669
		1186	1169	1643
	Days 1-3 versus Days 12-17	1327	1327	1326
		1513	1148	1416
		1159	1598	1680
		1533	1609	1624
		744	1529	1601
		1010	1510	1528

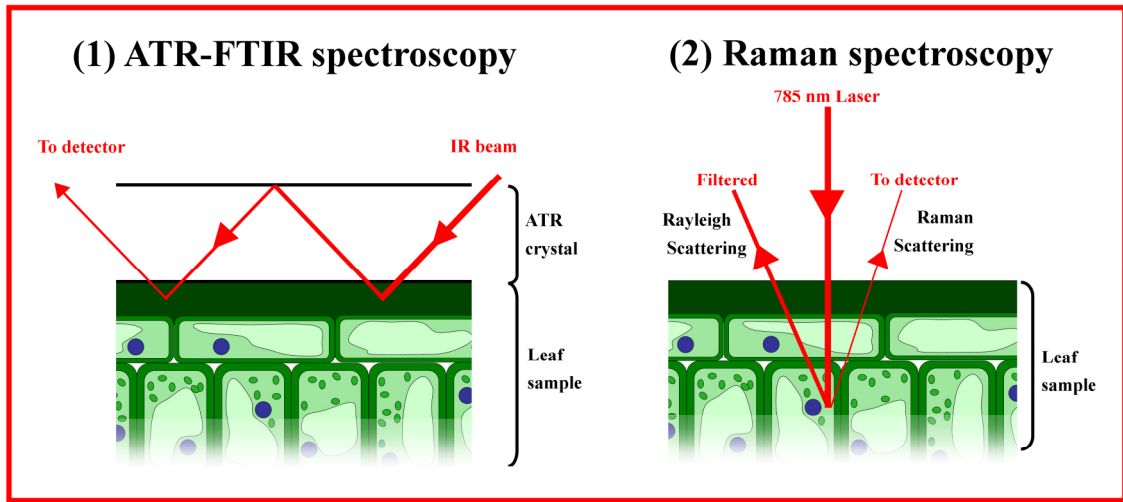
*Derived from one feature extraction technique.

Table 3. Top discriminating biomarkers as derived from feature extraction techniques, with tentative wavenumbers assignments derived.

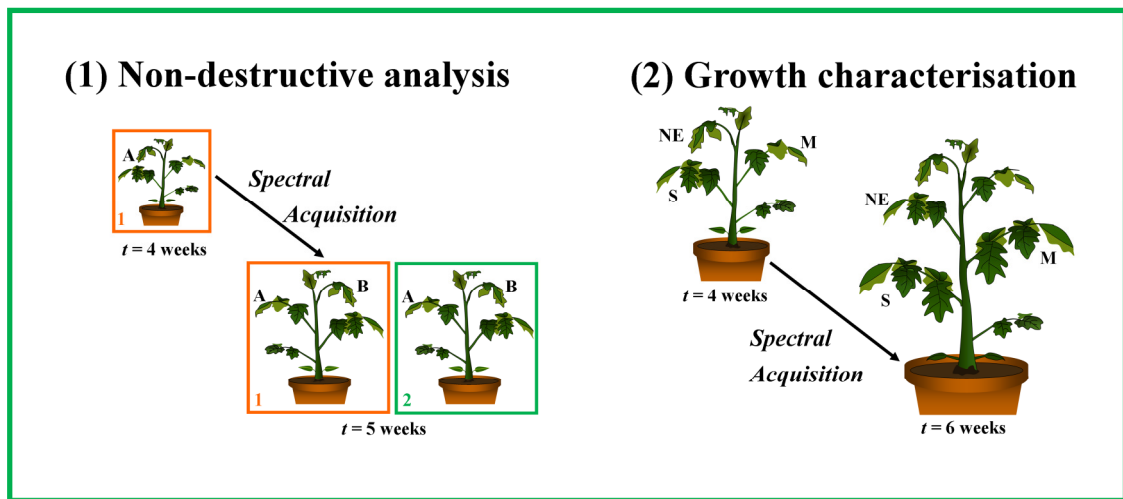
		<i>Wavenumber (cm⁻¹)</i>	<i>Tentative Assignment</i>	<i>Reference</i>
ATR-FTIR	Days 1-3	1408	CH ₃ deformation, $\nu_s(\text{COO}^-)$ in pectin	88
	versus	1512-1508	$\nu(\text{C}=\text{C})$ in lignin, carotenoid or protein	43
	Days 4-7	1107	$\nu(\text{CO})$, $\nu(\text{CC})$, pectin	32
	Days 1-3	1470-1466	CH ₂ bending in lipid	47
	versus	1308 - 1296	Amide III	80
	Days 8-11	1103	$\nu(\text{C-O-C})$ in ester	89
	Days 1-3	1647 - 1636	Amide I	61
	versus	1103 - 1099	$\nu(\text{CO})$ in cellulose	36
	Days 12-17	1015 - 1013	$\nu(\text{CO})$, $\nu(\text{CC})$, $\delta(\text{OCH})$, ring in pectin	34
	Raman	Days 1-3	1229 - 1217	Amide III
versus		1191 - 1173	$\nu_{\text{as}}(\text{PO}_2^-)$ in DNA	40
Days 4-7		1462	$\delta(\text{CH}_2)$ in hemicellulose	61
Days 1-3		1158-1157	$\nu(\text{CC})$ in carotenoid	90
versus		1328-1327	Chlorophyll	56
Days 8-11		1526-1527	$\nu(\text{C}=\text{C})$ in carotenoid	91
Days 1-3		1327-1326	Chlorophyll	56
versus		1159-1148	$\nu(\text{CC})$ in carotenoid	90
Days 12-17		1533-1529	$\nu(\text{C}=\text{C})$ in carotenoid, Chlorophyll	56

Figure 1

METHODOLOGY



IMPLEMENTATION



Analytical Methods Accepted Manuscript

Figure 2

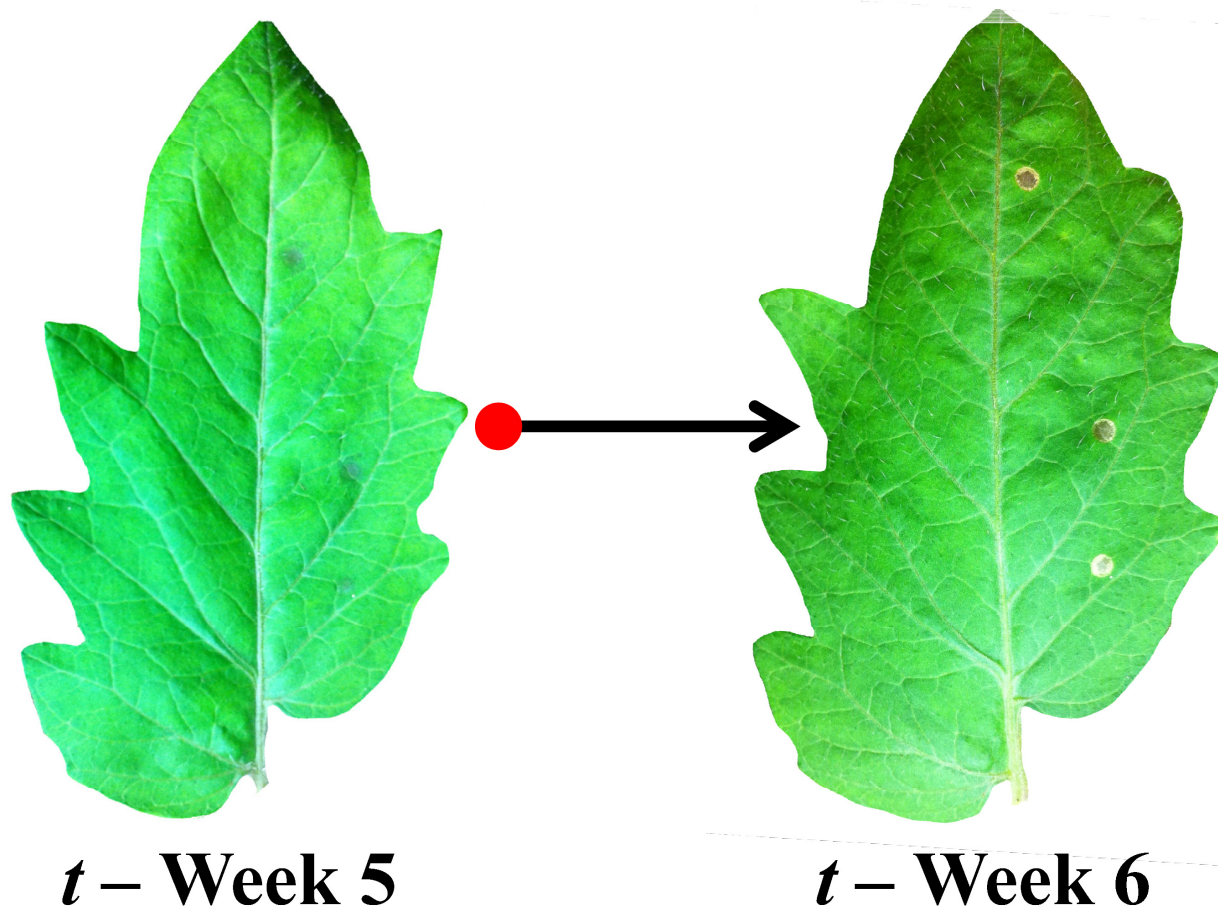
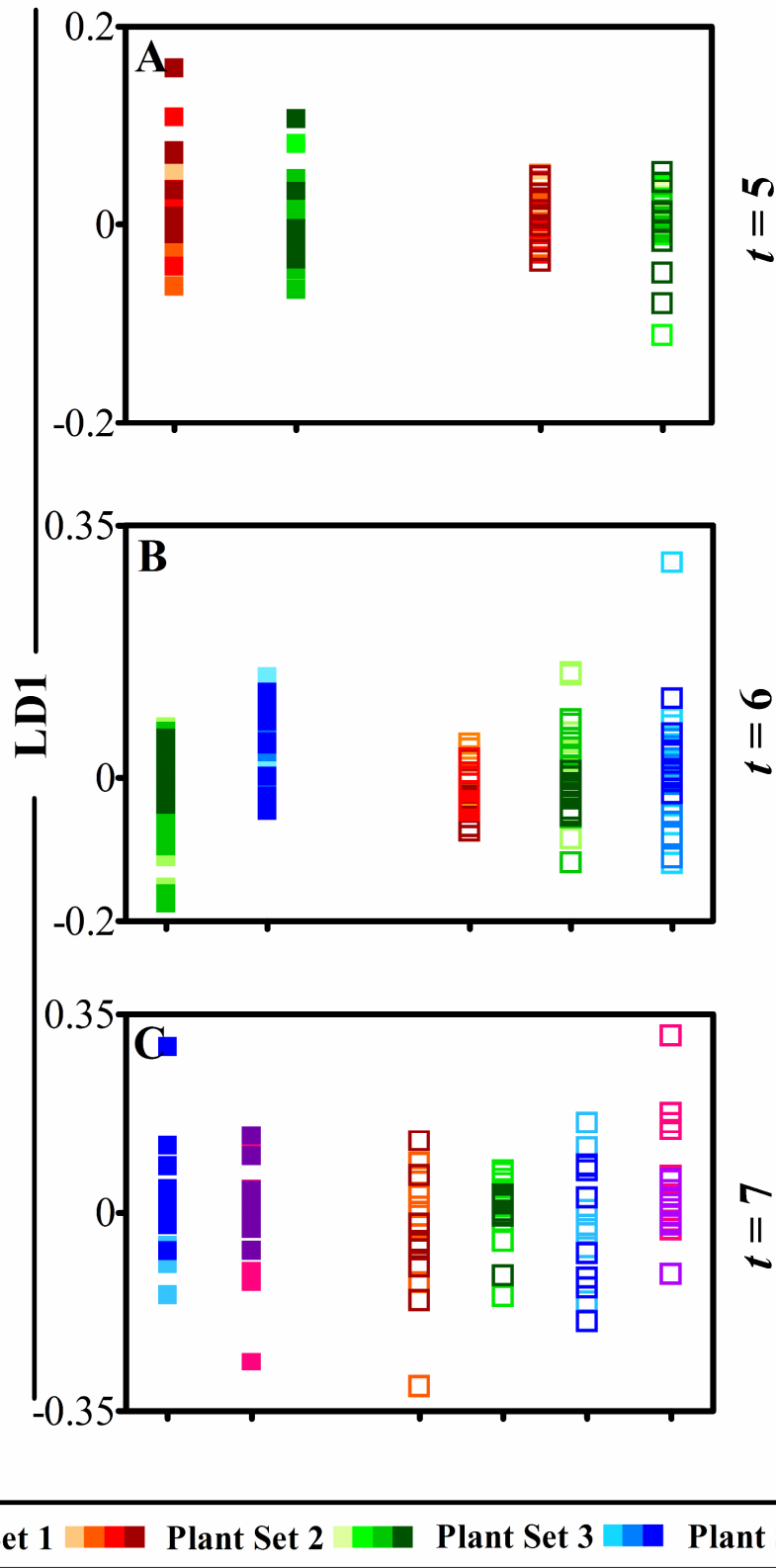


Figure 3



Analytical Methods Accepted Manuscript

Figure 4

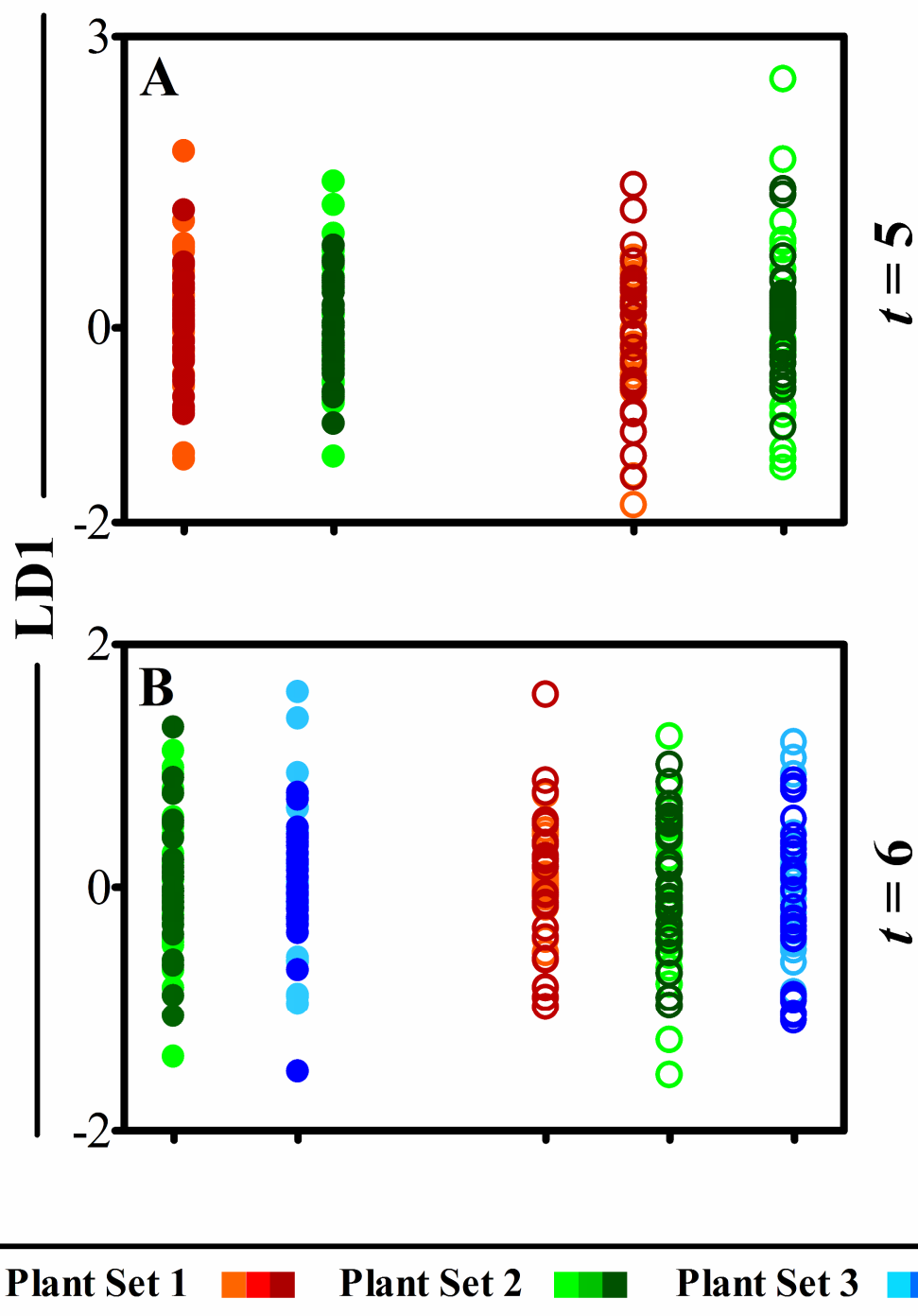


Figure 5

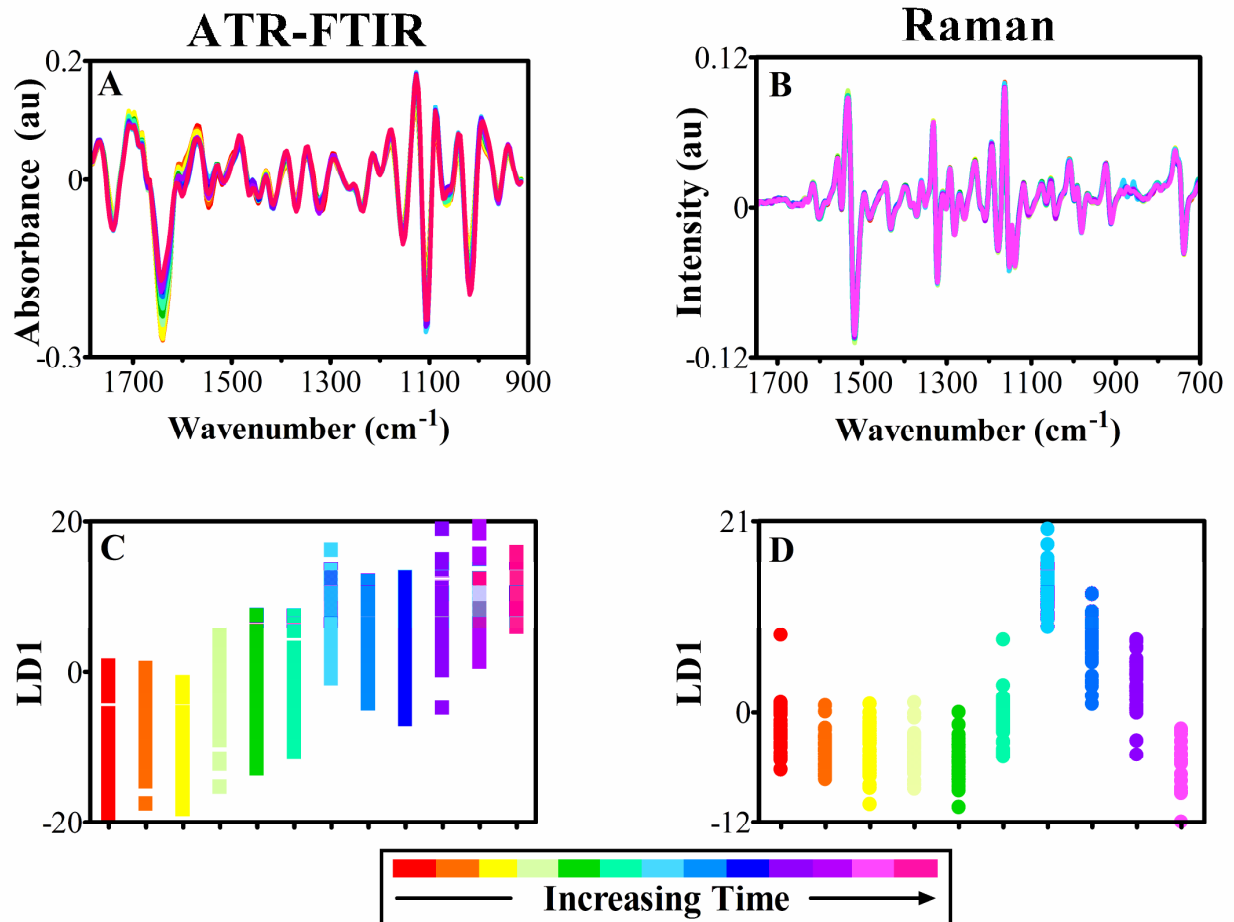


Figure 6

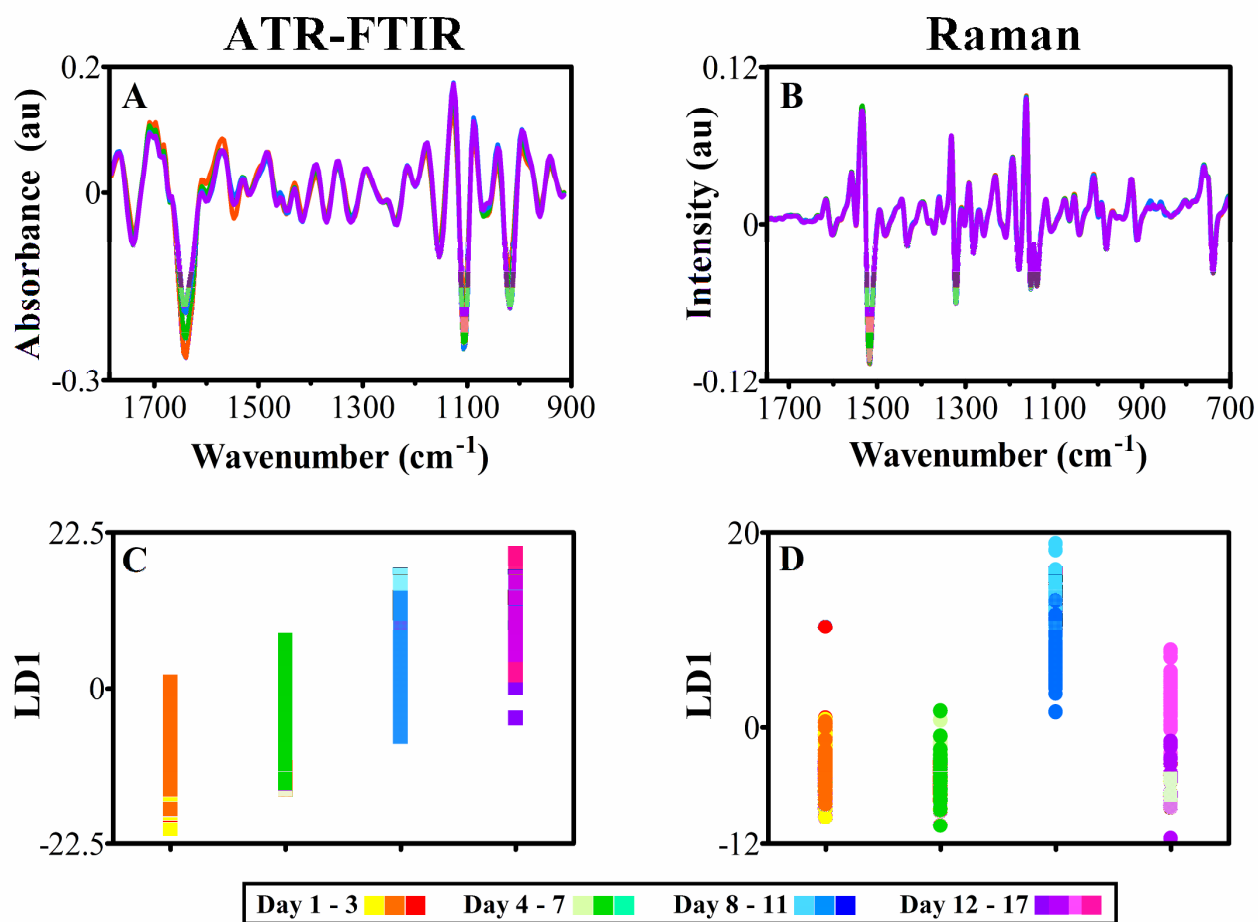


Figure 7

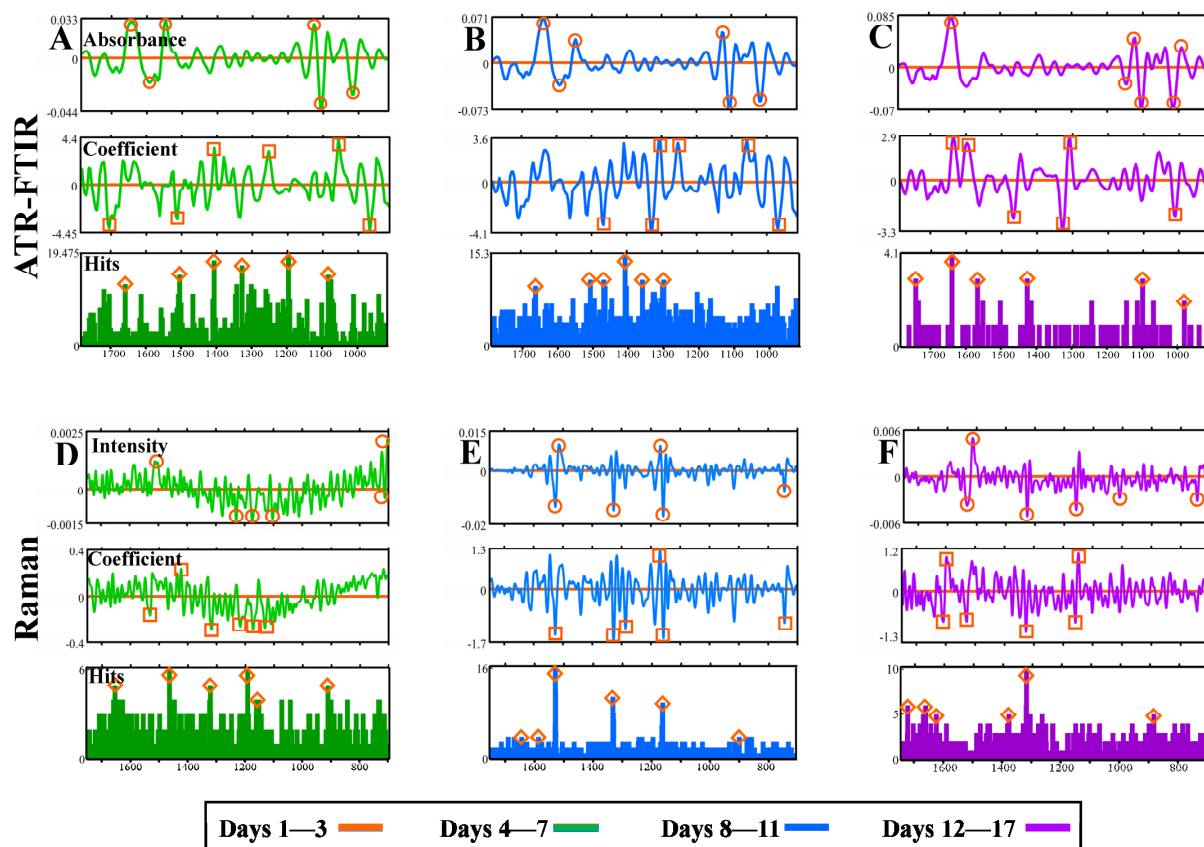


Figure 8

